Remote Sens. **2013**, *5*, 687-715; doi:10.3390/rs5020687

OPEN ACCESS

Remote Sensing

ISSN 2072-4292

www.mdpi.com/journal/remotesensing

Article

Flood Mapping and Flood Dynamics of the Mekong Delta: ENVISAT-ASAR-WSM Based Time Series Analyses

Claudia Kuenzer [1,*], Huadong Guo [2], Juliane Huth [1], Patrick Leinenkugel [1], Xinwu Li [2] and Stefan Dech [1]

[1] German Remote Sensing Data Center, DFD, German Earth Observation Center (EOC), German Aerospace Center (DLR), Oberpfaffenhofen, D-82234 Wessling, Germany; E-Mails: juliane.huth@dlr.de (J.H.); patrick.leinenkugel@dlr.de (P.L.); Stefan.dech@dlr.de (S.D.)

[2] Center for Earth Observation & Digital Earth (CEODE), Chinese Academy of Science, Beijing 100094, China; E-Mails: hdguo@ceode.ac.cn (H.D.G.); xwli@ceode.ac.cn (X.W.L.)

* Author to whom correspondence should be addressed; E-Mail: claudia.kuenzer@dlr.de; Tel.: +49-8153-28-3280; Fax: +49-8153-28-1458.

Received: 20 November 2012; in revised form: 1 February 2013 / Accepted: 1 February 2013 / Published: 5 February 2013

Abstract: Satellite remote sensing is a valuable tool for monitoring flooding. Microwave sensors are especially appropriate instruments, as they allow the differentiation of inundated from non-inundated areas, regardless of levels of solar illumination or frequency of cloud cover in regions experiencing substantial rainy seasons. In the current study we present the longest synthetic aperture radar-based time series of flood and inundation information derived for the Mekong Delta that has been analyzed for this region so far. We employed overall 60 Envisat ASAR Wide Swath Mode data sets at a spatial resolution of 150 meters acquired during the years 2007–2011 to facilitate a thorough understanding of the flood regime in the Mekong Delta. The Mekong Delta in southern Vietnam comprises 13 provinces and is home to 18 million inhabitants. Extreme dry seasons from late December to May and wet seasons from June to December characterize people's rural life. In this study, we show which areas of the delta are frequently affected by floods and which regions remain dry all year round. Furthermore, we present which areas are flooded at which frequency and elucidate the patterns of flood progression over the course of the rainy season. In this context, we also examine the impact of dykes on floodwater emergence and assess the relationship between retrieved flood occurrence patterns and land use. In addition, the advantages and shortcomings of ENVISAT ASAR-WSM based flood mapping are

discussed. The results contribute to a comprehensive understanding of Mekong Delta flood dynamics in an environment where the flow regime is influenced by the Mekong River, overland water-flow, anthropogenic floodwater control, as well as the tides.

Keywords: Flood; flood dynamics; flood progression; water detection; inundation; radar; Envisat; ASAR; WSM; feature extraction; time series; Mekong Delta; Vietnam

1. Introduction: Remote Sensing Based Flood Monitoring

Floods occur in many areas of the world and bring with them a range of negative but also many positive side effects. Every year floods cause numerous casualties [1]. In the last decade of the 20th century alone, about 1.4 billion people were directly or indirectly affected by floods and about 100,000 lost their lives [2]. According to the United Nations, more people lose their lives due to floods than due to any other natural hazard [3]. Unwanted inundation leads to the destruction of infrastructure and harvests and limits access to natural resources.

At the same time, floods and frequent inundation can be accompanied by positive side effects. Floodwaters contain nutrient-rich sediment fertilizing floodplain soils. Furthermore, inundated areas are habitat for fish and other aquatic animals. Floodwaters—when controlled, channelled, or stored—support long term water supply, irrigation activities, or even electricity generation. The monitoring of flood events, therefore, is a crucial task in earth observation. *In situ* assessments of flooded areas are usually difficult to undertake, and airborne or space-borne observations are the only realistic choice for continuous monitoring of large flooded areas [4].

According to numerous studies, e.g., [5,6], Synthetic Aperture Radar (SAR) provide the most suitable data for this endeavour, as cloud cover during the rainy season obscures optical observations. According to Leinenkugel *et al.* [7], cloud cover for the Mekong region reaches approximately 85%–95% in the rainy season, thereby making remote sensing analyses on the basis of optical image data a very challenging task. Radar systems, in contrast, enable data acquisition independent of weather conditions and time of day, as microwaves pass through most clouds, rain fields, water vapour, and aerosols. Flooded areas have very characteristic backscattering properties in radar images. As undisturbed water surfaces act as specular reflectors for incident microwaves, flooded areas yield no or a very low return signal, and can thus clearly be distinguished from open soil, vegetated agricultural land, forest land, or settled land [8].

However, influences of wind (leading to waves and hence increased surface roughness), extreme sediment load, or vegetative components in or covering the water can have impacts on the signal as well. A standard literature reference for the impact of forest canopies above flooded surfaces is Richards *et al.* [9]. They underline that C- and X-band data will usually not penetrate a tree canopy, and the return of a suitable L-band signal from a water surface below forest also depends on incidence angle, trunk geometry, and stand density. However, even with L-band data flood detection under canopy is usually not fully satisfactory. Hess *et al.* [10,11] employed SIR-C [10] and 100 m resolved

JERS-1 L-band data and achieved flood detection user accuracies of 62% in the low water stage of the Amazon, and of 86% during the high water stage. The area covered in this latter study was extensive.

Furthermore, very small observation angles can hamper water detection [4], and polarization of the incident radiation also plays an important role, as elaborated by Henry *et al.* [12]. They compared flood mapping results of Envisat ASAR Image Mode and Alternating Polarization Mode with ERS-2 derived flood maps and Landsat ETM+ derived ground truth. They found that HH polarized data is best suited for flood area discrimination and superior to HV and VV data. However, if HV is available jointly with HH data, the result can be further refined. VV polarized data is least suitable, as it is strongly influenced by surface roughness. This was confirmed in numerous studies, amongst others by Gstaiger *et al.* [13].

The above effects are also reviewed by Pierdicca *et al.* [14], who employed Italian COSMO SkyMed data for semi-automated flood detection in numerous case study sites located in Italy, Pakistan, Albania, Thailand, and Australia. These authors also underline the impact of microwave frequency on water detectability. While X-band as well as C-band data cannot penetrate into a forest canopy, L-band data has an increased capability to penetrate down to water surfaces which might exist below forest. Here the chance for a water-related return signal (if the stand is not too dense) is definitely higher than for X- or C-band data. Pierdicca *et al.* [14] also state that detailed local knowledge of an area (land cover, terrain, typical flood patterns) definitely helps to improve and interpret the flood mapping result and addresses the trade-off between semi-automated methods involving more human interaction (maybe even manual threshold selection) yielding very high accuracy *versus* fully automated rapid mapping approaches.

Methods of flood area extraction—or so called "water mask" derivation—are numerous and have been presented by several authors. Matgen *et al.* [15] have been working in the field for many years, and conclude that hybrid methodologies combining radiometric thresholding with region-growing approaches are the future pathway towards SAR based automated flood monitoring. Pulvirenti *et al.* [16] presented a fuzzy-logic approach considering three scattering models, simplified hydrologic assumptions and context information. Based on available pre-flood data their algorithm has the capability to detect not only open water areas, but also flooded areas beneath vegetation senescence. Martinis *et al.* [17,18] developed an automatic near-real-time flood detection tool for very high resolution TerraSAR-X SAR data combining split-based histogram thresholding and segmentation based classification. Although results are convincing, a challenge to this approach is that costly licensed software (Definiens Developer) is needed for the segmentation of the radar images. Mason *et al.* [19,20] also focus on high resolution TerraSAR-X data, presenting a semi-automated algorithm for flood detection in urban areas, addressing the problem of floods in settled regions which might be obscured by layover and foreshortening or radar shadow. This specific issue—while in general of high interest—is not so relevant for the data and observation scale addressed in this paper.

With respect to applications, the observation of flooded areas is usually undertaken based on multi-temporal data. Kuehn *et al.* [21] employed three Radarsat-1 data sets as well as optical Aster data for flood mapping in the Ganges Delta in Bangladesh. Hoque *et al.* [6] utilized multi-temporal optical and SAR data for flood monitoring in Bangladesh, Henry *et al.* [12] analysed one multi-polarized ASAR data set, and Schumann *et al.* [22] focus on future flood modelling using SAR data for surface roughness derivation. Pulvirenti *et al.* [23] analysed the flood situation after the 2011

Tsunami hitting Japan using COSMO SkyMed data. Some of the numerous examples for published flood related studies based on SAR data appear in [24–31]. However, for method studies as well as for application oriented studies larger time series are hardly ever studied. For method studies focussing on novel or improved tools for flood detection, usually a pre-flood image, a further image acquired during the flood event, as well as (possibly) a post-flood image are sufficient. In many application studies only two data sets (pre-flood, flood) are compared. Publications on flood dynamics and floodwater progression over a longer time period are rare, and for the Mekong Delta in Vietnam little is available.

In the Mekong Delta, Sakamoto *et al.* [32] detected temporal changes in the extent of annual flooding based on mainly optical 500 m resolved MODIS data spanning the years 2000–2004. In the field of radar based analyses, Long *et al.* [3] used five ERS-2 SAR data sets to map flood occurrence. However, so far flood patterns in the Mekong Delta have never been analysed with a radar based time series at a resolution of 150 meters, as we present here. A challenge of the delta is its more or less completely flat topography. Ancillary data like a DEM cannot support the refinement of flood detection. The questions which we aim to answer are the following:

- Which spatial patterns exist with respect to flood occurrence?
- Which areas in the Mekong Delta are most frequently flooded and why?
- Which areas in the Mekong Delta are not affected by floodwaters and why?
- How do floodwaters in the Mekong Delta progress over time?
- Which similarities or differences in floodwater dynamics exist between the observed years?
- How do artificial dikes impact flood patterns in the delta?
- What are the advantages and disadvantages of Envisat ASAR WS based flood monitoring?

2. Study Area: the Mekong Delta

The Mekong Delta in southern Vietnam with 39,000 km^2 is one of the largest river deltas in the world and home to over 18 million inhabitants. It is located between 8°30′–11°30′N and 104°30′–106°50′E and is the vulnerable end of the Mekong river [33] (see Figure 1). The Mekong originates at the Tibetan plateau and crosses China, Myanmar, Laos, Thailand, and Cambodia before entering the territory of Vietnam. The Mekong's discharge of 475 km^3/year makes it to one of the world's largest single-peak pulsing rivers [34]. Severe flood-pulse changes are expected to occur in the future due to regulatory measures (e.g., hydropower dams) upstream [33].

The delta—mostly located at an elevation well below 10 m above sea level—developed via thousands of years through the accumulation of fertile sediments [33,35]. Over 90% of the 13 Vietnamese provinces comprising the delta are located well below 3 m above sea level. The flat and open delta is often termed the 'rice bowl of Vietnam'. Rice production yields two, and in some areas up to three harvests per year [32,36,37].

Just recently, a detailed work examining rice cropping patterns in the delta based on hyper-temporal SPOT NDVI data was presented by Thi Thu Ha Nguyen *et al.* [36]. However, especially the coastal areas of the Mekong Delta are increasingly being converted to aquaculture areas. Shrimp ponds extend all the way to the coast and lead to the depletion of the last remaining forest fragments of coastal mangroves or other natural vegetation protecting the coast [38,39]. Overall, the delta is mainly dominated by seasonal agricultural land use, and tree cover is very limited. Tree cover occurs as slim

belts of mangroves along the south-western coastline, and as fruit tree orchards in the southern centre of the delta. The region experiences prominent dry and rainy seasons influenced by the south-west Indian and north-west Pacific monsoon. The dry season lasts from late December to May, while the rainy season (causing most of the 1,800 mm of precipitation in the area) usually lasts from early June to December. During the rainy season, large areas of the delta are flooded and fertilized by about one billion m^3 of sediment [36]. Thus, the people living in the delta call the annual flood 'the beautiful flood' [40]. They have learned to live with frequent flooding, as floodwaters are indispensable for the delta's agriculture [41]. Furthermore, inundation allows for seasonal fishing. Extreme events leading to fatalities are relatively rare, but occurred in 1961, 1978, 2000, 2001, and 2002, whereby each event was accompanied by the death of several hundred people, many of them unable to swim [40]. The hydrodynamic conditions in the delta are strongly altered by over 55,000 km of man-made canals [42]. Figure 1 depicts an overview of the area.

Figure 1. The study area: the Mekong Delta and its 13 Vietnamese provinces in southern Vietnam. Here the Mekong splits into nine branches before reaching the South China Sea.

Major challenges in the delta in recent times can be attributed to socio-economic transformation and urbanisation processes [43] leading to the degradation of the last natural forest and wetland areas [38,39], accompanied by increasing water pollution. Furthermore, climate change is a threat. The delta is one of the most endangered places on Earth with respect to sea level rise. Rising sea levels are forecasted to lead to intensified saltwater intrusion into the Mekong main stems and canals, as well as into aquifers and soils, as tidal saltwater influences progress further inland [40,41,44,45]. According to an IPCC prognosis (2007) of sea level rise between 75 and 100 cm by the end of this century, about 20%–50% of the low lying delta will be affected if no countermeasures are taken. Currently, ocean-induced flooding mainly plays a role during tropical storms and typhoons, which are expected to increase in frequency [40]. In the Mekong Delta, the flood regime is defined by a complex mix of four

influencing factors. Type 1 floods are mainly induced by the flood pulse of the Mekong as well as overland flow. Type 2 floods are artificial floodwaters distributed via a dense network of canals and controlled by dykes and sluice gates. Type 3 floods are short-term floods due extreme local precipitation events. Type 4 floods are mainly related to high tides during storms. Usually, no single flood occurrence in the Mekong can be solely assigned to one of the four factors. Instead, flood occurrences are always triggered by a combination of several of the four sources (see Figure 2). This complexity has already been introduced and discussed by Nguyen Viet Dung [35], Vo Khac Tri [46], Apel *et al.* [47], and Delgado *et al.* [48].

Figure 2. Typical flood regime depictions of the Mekong Delta, Vietnam. **Upper left**: Small canal with permanent water used for transport. **Upper centre**: Banks of canals are usually vegetated, and water may occur beneath vegetation. **Upper right**: Typical small dyke, which borders a large flooded area. **Middle left**: Overland flow. Large areas are flooded. **Middle centre**: At this stage flooded fields are used for fishing. **Middle right**: pumping excess water from field into the canal at a higher level. **Lower left**: Floodwaters have mostly retreated from this agricultural field. **Lower centre**: Large rice fields have been freshly planted. **Lower right**: The rice is heading, fields are slightly irrigated. (All photographs taken by C. Kuenzer in the Mekong Delta, November 2011).

3. Available Satellite and Ancillary Data

On 1 March 2002 ESA's Envisat satellite was launched, and data from sensors like ASAR (Advanced Synthetic Aperture Radar)—operating at C-band—were available until Envisat operational services ceased in April 2012. Envisat ASAR data come in different modes with different spatial resolutions and coverage. Data is available in Image, Wave, and Alternating Polarisation modes at approximately 30 m × 30 m in the highest resolution, approximately 150 m × 150 m in Wide Swath Mode (WS), and at 1 km pixel resolution in Global Monitoring (GMM) mode. Data from Envisat ASAR can be obtained via ESA's science programme. Since ESA approved a new data policy in May 2010, ESA's Earth Observation Data could be accessed mostly free of charge via the submission of a project proposal for research applications. We obtained all data (archived as well as scheduled, whereas scheduling often collided with other requests) in ASAR WS mode (WSM), which has a swath width of 400 km, and 150 m pixel spacing. Not all of the data were exclusively available for the rainy season. In the context of the present study, the following Envisat ASAR WSM data sets were available for the consecutive years 2007, 2008, 2009, 2010, and 2011 (see Table 1):

Table 1. Envisat ASAR WSM data sets available for monitoring inundation in the Mekong Delta. Scenes acquired during the rainy season appear in bold letters.

2007	2008	2009	2010	2011
2007-06-14	2008-06-01	2009-06-02	2010-01-14	2011-01-03
2007-07-03	2008-06-17	2009-06-18	2010-01-17	2011-01-14
2007-07-10	2008-06-24	2009-07-04	2010-02-18	2011-02-02
2007-07-19	2008-07-03	2009-08-27	2010-03-25	2011-03-04
2007-08-07	2008-07-22	2009-10-01	2010-04-29	2011-03-15
2007-08-14	2008-08-14	2009-12-10	2010-05-02	2011-04-03
2007-08-23	2008-08-23	2009-12-13	2010-06-03	2011-06-21
2007-09-11	2008-08-26		2010-07-08	
2007-09-18	2008-09-11		2010-08-12	
2007-10-16	2008-09-30		2010-08-15	
2007-10-23	2008-10-07		2010-09-16	
2007-11-01	2008-10-16		2010-10-08	
2007-11-20	2008-11-04		2010-10-21	
2007-11-27	2008-11-11			
2007-12-06	2008-11-20			
	2008-11-23			
	2008-12-16			
	2008-12-25			

ASAR has a repetition rate of 35 days. However, more than one path can be used to cover the Mekong Delta. We used mainly archive data for our analyses and ordered all the data available in the archive, which led to approximately two to four coverages per month. As a window for our data search we defined June to December (rainy season in the Mekong Delta); however, in 2010 and 2011 other dates were also retrieved from the archive. Unfortunately, in 2009 and 2011 less data were available in the archive due to the acquisition of alternative ASAR modes (WSM cannot be tasked in parallel).

However, despite these restrictions, we could build up a comprehensive time series of over 60 ASAR scenes located over the Mekong Delta. Additional data available for this study included the MEKONG LC2010 map, a MODIS time-series-derived land cover/land use classification generated by Leinenkugel *et al.* [49], as well as different vector data sets, such as province boundaries.

4. Methods and Data Analyses

All radar amplitude data were firstly geo-corrected using the open source software package BEAM, provided by the European Space Agency ESA. The flooded/inundated areas were then derived from the radar amplitude data, as briefly explained below, and in depth in Huth *et al.* [50] and Gstaiger *et al.* [13].

One main goal of water mask processing is the rapid and repeated delivery of Mekong Delta flood information over the course of several years in the context of the large German-Vietnamese WISDOM project (Water related Information System for the Sustainable Development of the Mekong Delta, [51,52]). Therefore, a main requirement for the algorithm used for data processing is simplicity and speedy performance, applicability to different types of radar data (not relevant for this paper, but a determinant for algorithm choice), independence of expensive licensed software, and availability as an embedded web processing service (WPS).

A simple threshold method enables the separation of water pixels, represented by low backscatter values, from non-water pixels, which usually have higher values in the image histogram depicting backscatter distribution. As laid out in Gstaiger *et al.* [13], to firstly reduce the typical speckle typical for SAR imagery, the first step of the algorithm is to apply a standard convolution median filter with a kernel size of 5 × 5 pixels, resulting in a filtered and speckle reduced image P1. After this pre-processing two empirically chosen thresholds divide water from non-water pixels (processed image P5). Here, the first threshold, T1, which has a lower value than the final water threshold, defines confident water areas, leading to P2. The second threshold T2, which has a higher value than the land threshold, classifies confident land areas, leading to image product P3. Then buffer zones of two pixels, which are only generated via dilatation, are applied to P", which results in product P4. The buffers define the transition zone from water to land, also represented by mixed pixels. The second threshold now enables the inclusion of the water pixels within this zone in the initial binary water mask. The temporary results P3 and P4 are now compared, and if coincidence occurs the value (water or land, 0 or 1) is written to P5. Otherwise, the value from P2 is written to P5 (P4 & P3 || P2). In this way overestimated water pixels are excluded. Proceeding further, isolated pixels are removed via morphological image closing (P6) [13] (see Figure 3). The removal of so-called 'islands' and 'lakes' according to a defined maximum size (T3,T4) is mainly of relevance for higher resolution SAR data (e.g., TerraSAR-X data also processed in the course of the project), but does not affect Envisat ASAR derived results at 150 m resolution.

The results of this algorithm have been compared with other flood mask derivation approaches—e.g., a histogram texture based approach, and a very interactive object based approach—and it was found that the accuracies of the approach which we use here (97.6%) and the very interactive object based approach (97.8%) were more or less the same, and exceeded the accuracy of a further texture based approach tested (95.6%) [13].

Figure 3. Processing chain of the histogram based approach for water mask derivation (modified from Gstaiger *et al.* [13]).

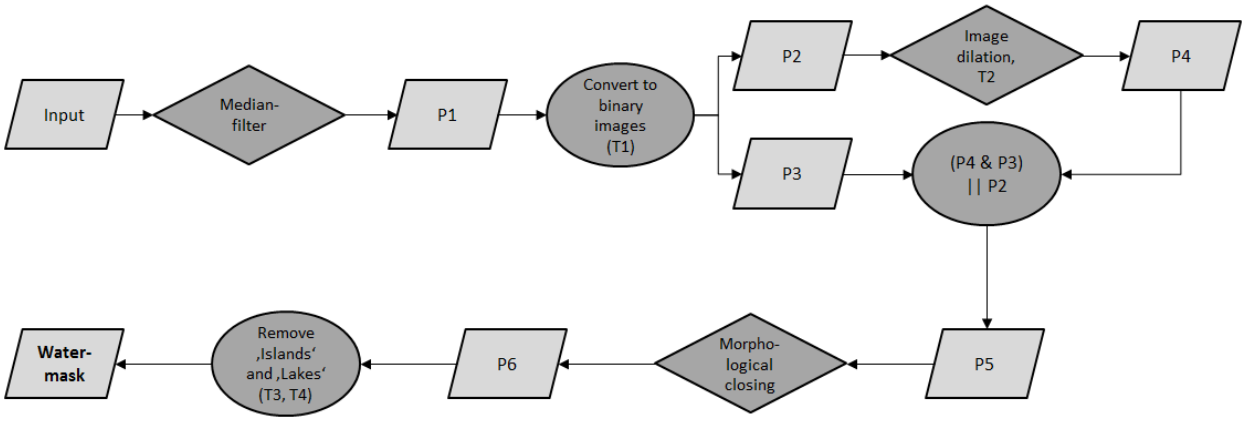

Furthermore, our algorithm enables automatic processing of the water masks right at data delivery via email by the data provider and up until integration of the product in a web-based information system for the Mekong Delta [53]. The water mask processing chain combines all processing steps from data retrieval to product generation, and data ingestion and all steps have been encapsulated in a Web Processing Service, WPS, allowing for fully automatic processing [13,54].

The algorithm for water surface extraction yields products of high accuracy, and derived flooded areas have been validated indirectly via comparison with high resolution optical and TerraSAR-X data and *in situ* ground surveys of water-land boundaries [13]. Considering that the ASAR WS data have a rather coarse resolution of 150 metres, the land-water boundary cannot be determined anyway down to metre accuracy. We employed the algorithm to derive so-called 'water masks' for our study region. Processing yielded the water masks for the individual time steps available as binary 0/1 files (no water/water) for each individual scene (see Figure 4).

Figure 4. Original ENVISAT ASAR WSM radar image for 2007-06-14 (**left**), and water mask derived for 2007-06-14 (**centre**). The differing extent of flooding between the start of the rainy season (centre) and the flood peak around the end of the rainy season (**right**) is evident. Extent: UL: 12°N, 104°15′E, LR: 8°30′N, 106°50′E.

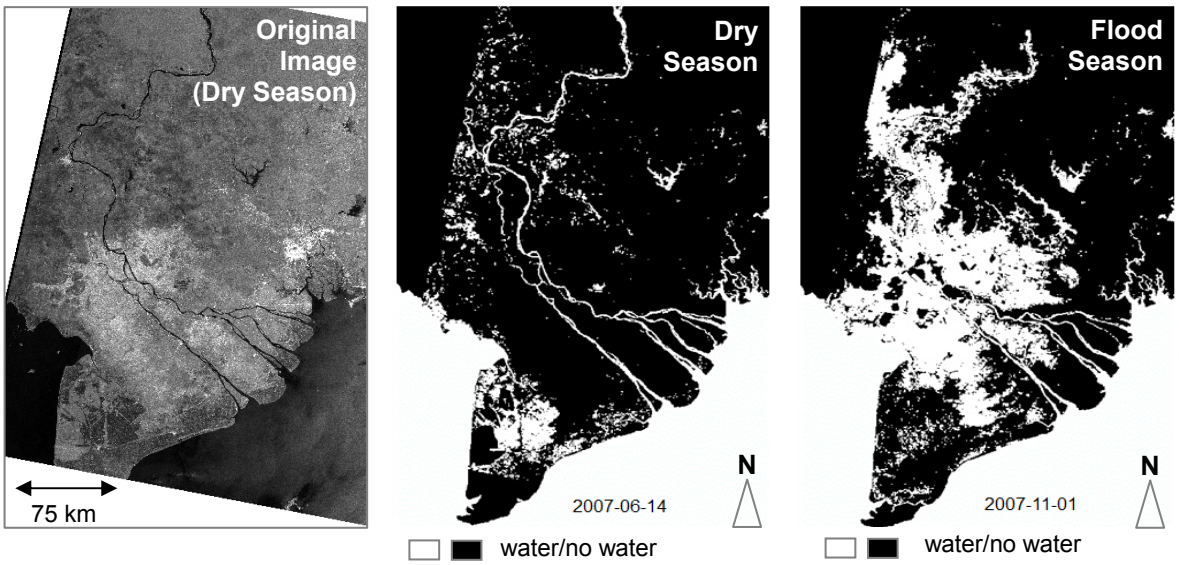

Water masks for each year (e.g., 2008) were summed up to obtain an image product depicting how many times an area was covered with water during the respective rainy season within that year. This enables an understanding of flood length for different areas. Furthermore, all sum products for the individual years (*i.e.*, ASAR 2007, 2008, 2009, 2010, 2011) were added to retrieve a long time series of water covered (flooded) *versus* non-flooded areas, which happens to be the longest SAR-based time series of flood occurrence for the delta.

Since the footprints of many scenes did not completely overlap, but only shared a certain region in common, a so-called 'largest common coverage', LCC, footprint was generated. This LCC footprint was derived for each individual year, as well as for all years, to enable later statistical analyses within the years, as well as for the five-year time-span in regions of comparable coverage only. This LCC approach ensures that we do not compare areas which were covered by a varying amount of data acquisitions over the year. This process flow is depicted in Figure 5.

Figure 5. Derivation of flood occurrence (summed) for individual years or all years, considering the largest common coverage (LCC) of all scenes. Data processing procedure; exemplary binary water mask for one time step; creation of the largest common coverage based on radar scene footprints. Extent of lower left image: UL: 12°N, 104°15′E, LR: 8°30′N, 106°50′E.

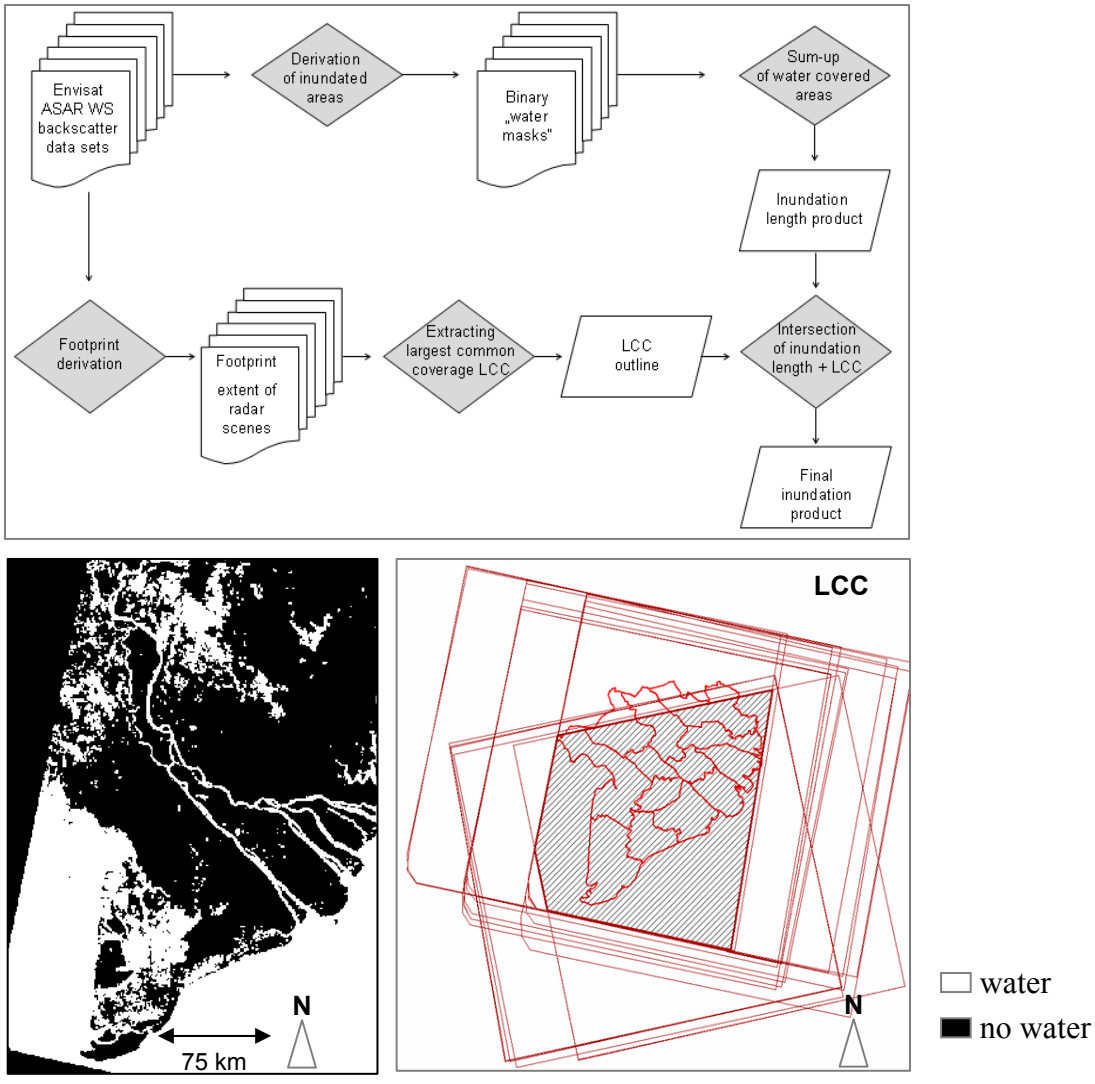

5. Results

5.1. Floodwater Occurrence and Progression for One Selected Year (2007)

Figure 6 presents the flooding regime over the rainy season for the year 2007. This year was chosen for display since the largest common coverage for this year (within red boundary) is larger than those for 2008, 2009, 2010 and 2011 and therefore depicts typical patterns best. The year 2007 was neither an extreme flood year nor a drought year. As listed in Table 1 and depicted in the figure, the time span between 14 June and 6 December is covered.

Figure 6. Floodwater distribution during the 2007 rainy season, depicted only for the largest common coverage. Each subset contains the exact date and flood percentage. Image extent: LL: 8°46′50″N, 104°35′05″E, UR: 10°55′50″N, 106°29′26″E.

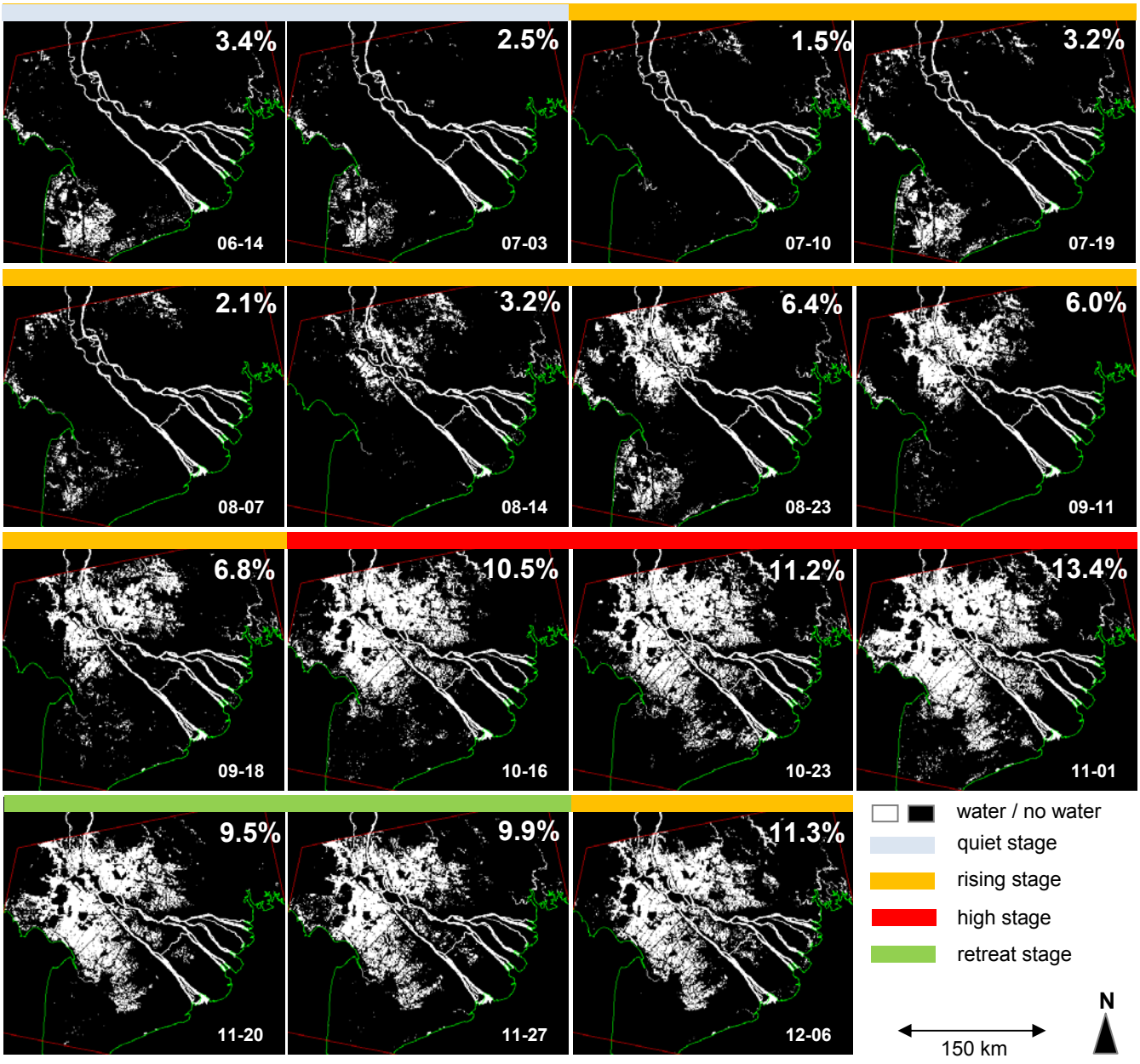

We can observe a clear rising stage of floodwaters (orange), where water progresses from north to south. River-induced and overland flow (type 1 flood) as well as human control (type 2 flood) are the main causes for the spread of inundation (orange). During the high stage (red) the flood area covers more than 10% of the observed area and a slight progression is still recognizable. From November onwards floodwater retreated back, from south to north, and radially from areas further away from the main stem to areas closer to the river. However, in December floodwaters unexpectedly rose again. Flood variability in the south-western tip of the delta (Ca Mau province and neighbours) is not related to the type 1 flood dominating the northern part. Instead, in the very lowest lying part of the delta flooding is mainly induced by the tide (type 4 floods) and human control (type 2 floods) [35,42,55]. Extreme rain events in the delta (type 3 flood) can occur at any time in the rainy season, and lead to short-term patches of shallow water [47]. According to Nguyen Nghia Hung *et al.* [42] and Delgado *et al.* [48] the flood hydrograph (as measured at *In situ* gauge stations at the northern border) in the delta is characterized by two peaks: the first between mid-July to mid-August, and the second between September and October (note the sharp increase between 08–14 and 08–23, as well as between 09–18 and 10–16).

5.2. Flood Frequencies for 2007, 2008, 2009, and 2010

Figure 7 below presents the results of the added flood occurrence (sum) products for the years 2007, 2008, 2009, and 2010. As only one acquisition during the rainy season (see Table 1) was available for the year 2011, this year is not presented in Figure 7. However, the years 2007 (already presented as an individual observation in Figure 6) and 2008, as well as 2009 and 2010 are covered with an about equal amount of rainy season data and are thus comparable—at least for the spatial areas covered by both of the respective data sets. The flood occurrence sum images are generated according to the flow chart depicted in Figure 5. Very bright (white) areas were flooded numerous times, while lower grey values indicate less frequent flooding. Images would look identical if they were normalized to per cent—however, in the legend we prefer to keep the number of available observations for better transparency. The figures have slightly different extents due to the varying largest common coverage, LCC. The long time series for 2007 and 2008 show a similar flood distribution: the areas most often flooded are the northern areas of the Mekong Delta, whereas the coastal areas are less affected by flooding. This is confirmed by the spatial profile, which cuts the delta along the orange line (2007) from north-northwest to south-southeast. A clear trend towards shorter flood durations when approaching the coast can be noted. This can also be observed for the 2008 subset. Since 2010 was an extreme drought year for the delta [56] it stands out that the northern flood plains are not as strongly flooded as in the previous years.

Figure 8 presents a more detailed illustration of the 2007 flood occurrence data set shown in Figure 6. Displayed at enlarged extent and in color, we can clearly depict flood occurrence patterns during the rainy season of 2007. Floodwaters remain for nearly all the rainy season in the northern delta; mainly in the provinces of An Giang, Dong Thap, northern Long An, and Can Tho. Within the northern region, areas which are not flooded are either elevated or strongly dyked, as will be presented later. Subset b) on the right side of Figure 8 depicts flooded fields in northern Can Tho province. The boundaries between the fields, usually paved road or dirt roads constructed on top of a dyke, are rarely flooded. Flooding here only occurs a very few times per year, when over-bank flow or very heavy rains lead to a sudden increase

in the water level of canals and on fields. The coastal province of southern Long An, Tien Giang, Ben Tre, Tra Vinh, and Soc Trang (see Figure 1) are hardly ever affected by type 1 or type 2 flooding.

Figure 7. Added flood occurrence (sum) images for 2007, 2008, 2009, and 2010. According to the largest common coverage, LCC, the subsets differ in extent, but are displayed at the same scale. The profile presents inundation frequency along the profile line depicted in the upper left figure of 2007.

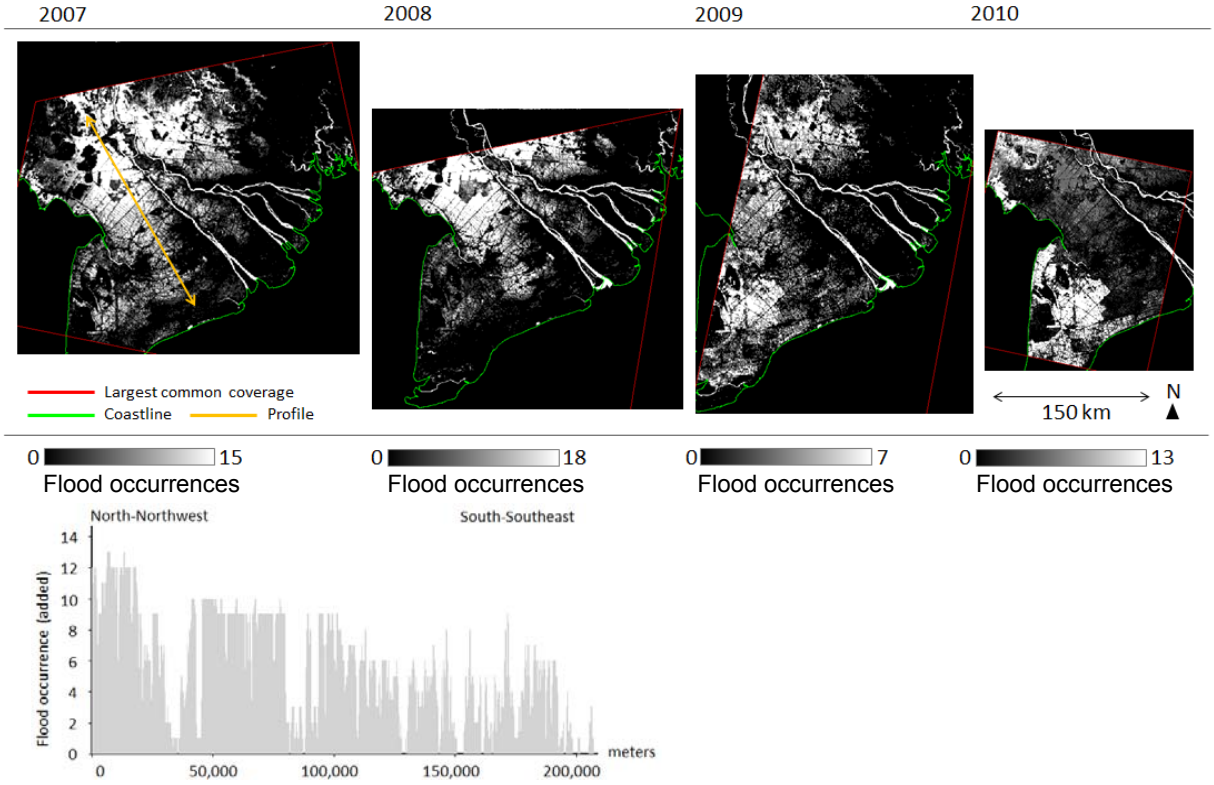

Figure 8. Flood dynamics in the Mekong Delta for the 2007 rainy season, based on 15 Envisat ASAR WSM derived water masks. Areas which are nearly always flooded are shown in reddish tones. The two zooms ((**a**) and (**b**)) depict flooded fields which are separated by dykes (elevated roads, pathways).

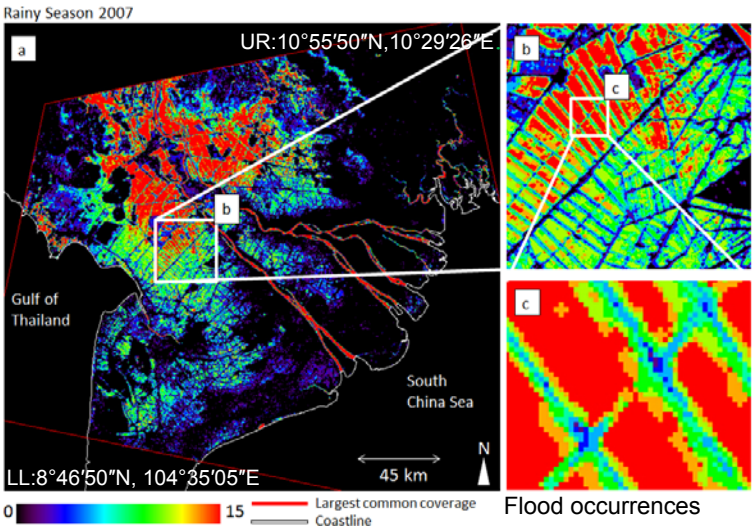

Figure 9 shows the inundation patterns in the Mekong Delta over the course of five years. Dark areas (except the ocean) were never, or only very rarely, detected as being flooded or inundated during the entire observation period, while coloured regions were inundated up to 58 times. Areas most frequently flooded during the rainy season are located in the northern and south-western Mekong Delta. The southern coastal provinces and the south-eastern areas, where the main stem splits up and reaches the south China Sea, are rarely flooded or inundated. It is furthermore obvious that the areas close to the main river arms are well protected by dykes, and extensive large-scale flooding and inundation rarely occur in the vicinity of the river banks. Another reason for limited flood detection is the fact that river banks as well as canals banks are usually vegetated with palm trees and other trees—with Envisat ASAR WSM data it is not possible to detect flooded areas beneath dense tree cover. In contrast, the main Mekong branches are depicted as water covered areas in nearly all observations. As the Mekong never runs dry, the river's main branches should actually be displayed as water-covered for the maximum time span (58 observations). However, a few times probably not all pixels within the river were declared as water—this can occur due to the extremely high sediment load, or strong wind (wavy water surface). Strictly speaking, only the area within the white boundary is covered by all 58 data sets. However, we present the whole delta, as general patterns are still valid. Several areas are rarely or even never detected as being flooded (see optical data snapshots in Figure 8). Except for the mangrove area, where floodwaters often exist below a dense canopy, this is reasonable.

Figure 9. Inundation in the Mekong Delta from 2007 to 2011 derived from all available Envisat ASAR WSM data. (**a**) hills in the Tri Ton District north of Chau Lang, (**b**) Tram Chim National Park, (**c**) well-dyked agricultural area north of Hon Dat, (**d**) the Can Tho Cuu Long Rice Research Institute test field, (**e**) the tip of Ca Mau province with dense mangroves, and (**f**) fruit tree orchards.

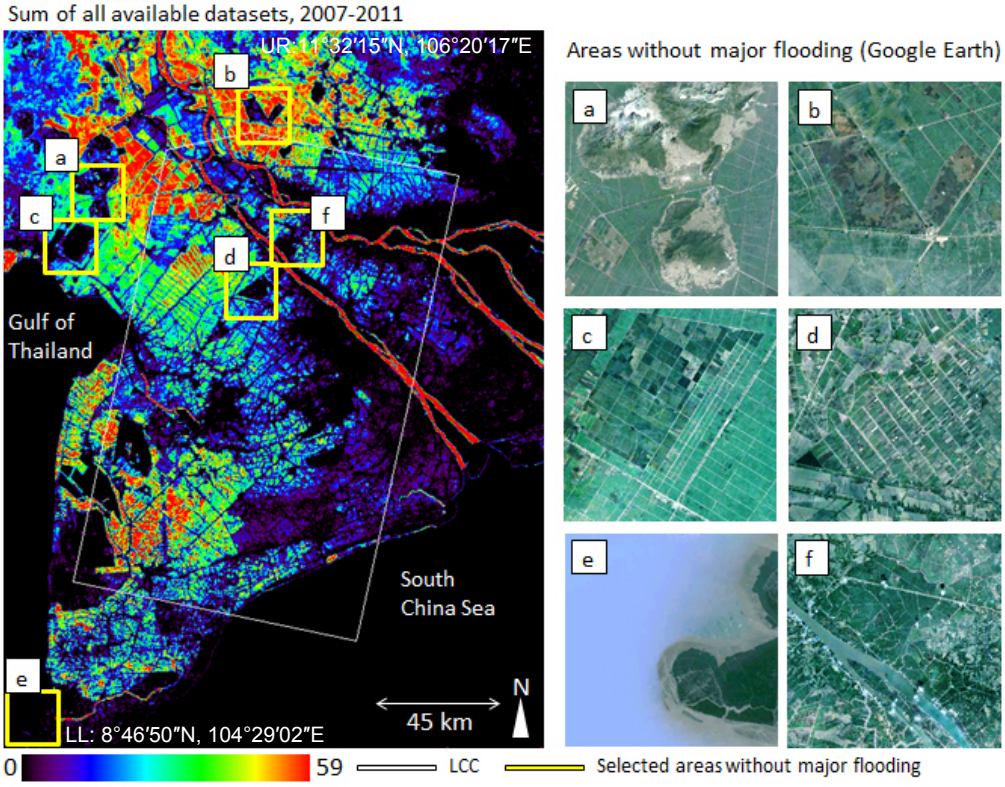

All distinct areas within the Mekong Delta which are rarely or never detected as being covered with water can be explained with local land cover and land elevation. For example, regions (a), (b), (c), and (d) are in fact never flooded (because located at too high elevation, or too well protected). However, tree covered areas (e) and (f) need some additional explanation. Regions where mixed fruit tree plantations dominate land use are usually also slightly elevated, and flooding in this area is very rare [46]. However, where *melaleuca*, *nypa* palms, and mangroves are prevalent, radar beams cannot pass through the dense canopy, and also here inundation below the trees cannot be observed.

The three diagrams in Figure 10 depict how much of the fully covered (LLC) provinces for the respective years are flooded. The figure enables an understanding of flood progression.

5.3. Overall Flood Progression and Comparison of Flood Progression for Selected Years

The diagrams below depict how much of the provinces were flooded during the respective day of the year when we observed them. Compared to—for example—Figure 6, Figure 10 enables a more quantitative comparison of flood progression. The x-axis presents the day of the year (DOY), and the y-axis displays how much (what percentage) of the province is flooded (1 = 100%). In 2007 Ca Mau was not included in the LCC. In 2008 Ben Tre, Long An, Kien Giang, Dong Thap, and An Giang are not fully covered and thus missing. In 2009 Ca Mau, Tra Vinh, Kien Giang, Dong Thap, and An Giang are not included. However, a comparison of the province areas fully covered during all three years is possible, and we do not want to withhold the information for the other provinces, as clear patterns can be observed.

Provinces located near the coast are displayed in darker blue, while the light blue plots represent provinces further away from the coast. For all three years provinces further away from the coast are flooded to a larger extent than were provinces near the coast. The only exception is the large flooded area at the very beginning of the rainy season in 2009 in Bac Lieu province. This flood event cannot be attributed to river or overland flooding (type 1), as in this case the northern provinces should show larger flood extents as well. The flooded area here may stem from coastal inundation after a very high tide, but this is only speculation.

Except for this outlier event, coastal provinces are usually flooded over not more than 0%–15% of their territory. In flood prone provinces such as An Giang, Dong Thap, and Can Tho above 40% of the province area can be flooded during the high stage. During the observation for DOY 305 in 2007 the three provinces were covered with floodwater to over 50%. In 2008 An Giang and Dong Thap were unfortunately not included in the largest common coverage, but floods in Can Tho again covered over 40% of the province during DOY 290.

Generally, all three graphs show that the flood area steeply increases after DOY 215 in 2007 and 2008. In 2009 floodwater increase starts earlier and does not seem to be as extreme, but in that year we have far fewer observations available. Both in 2007 and 2008 the high flood stage occurs roughly between DOY 275 and DOY 320. In 2008 the flood furthermore seemed to arrive via three strong pulses starting around DOY 236, DOY 274 and DOY 308.

Figure 10. Flood patterns during observed days of the year (DOY) for different fully covered provinces. Provinces displayed in darker blues are located on the coast, provinces in lighter blue further inland (the lighter the blue tone, the further north the location).

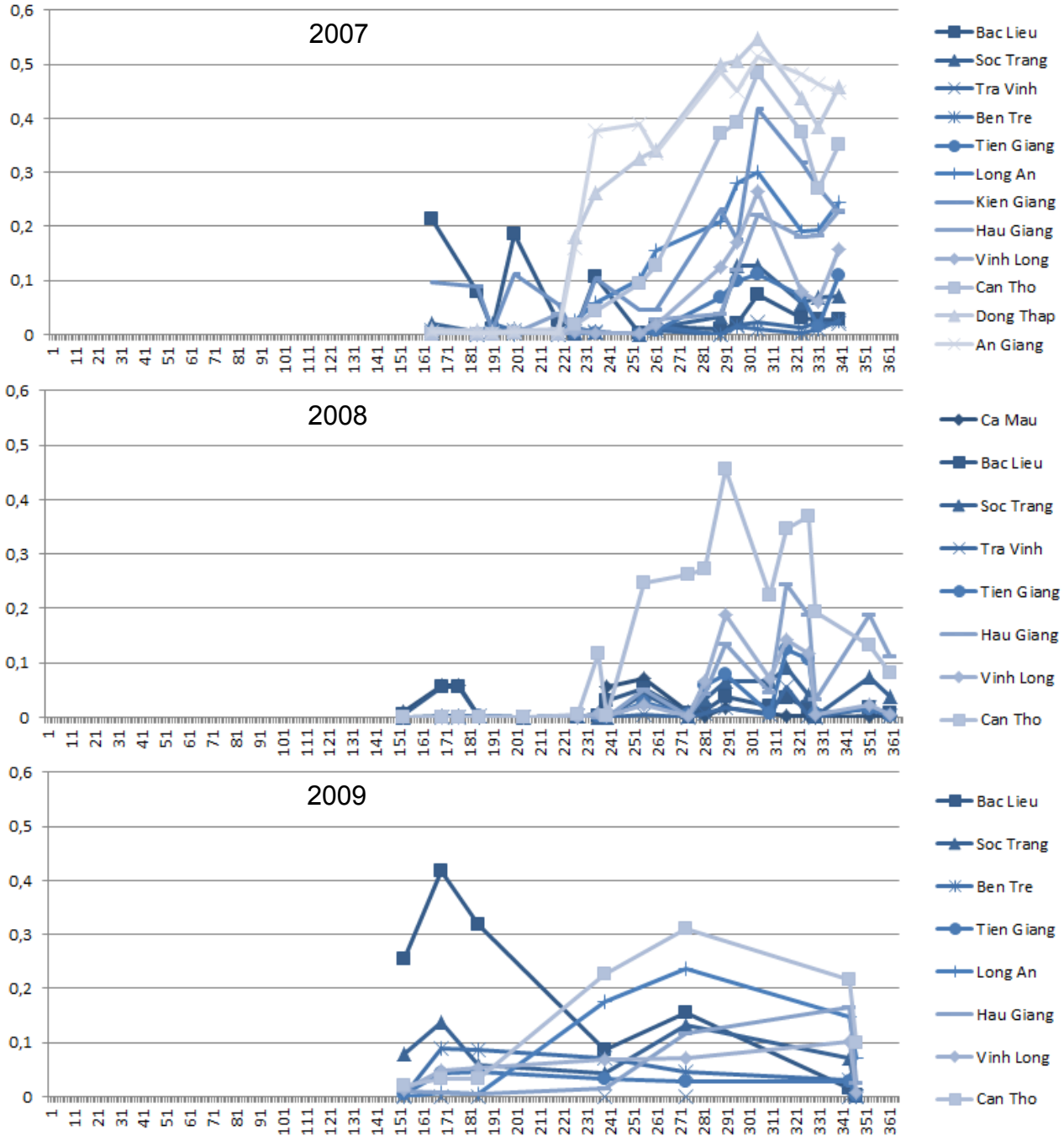

However, precise interpretation is difficult. The fact that four flood types (river/overland; human control, local rain events, as well as tidal influence) impact inundation in the delta makes it nearly impossible to separate the components—especially as we unfortunately had no detailed gauge station or hydrologic station data at hand. The time series could be interpreted at even greater detail if we had information available on typhoon landfalls (and the time lags for the accompanying rain events), extraordinary high tides and storms, as well as dyke control schemes. However, interpretation would then also exceed the scope of this remote sensing related paper.

Figure 11. Flood progression in the delta in 2007 (**upper**) and 2008 (**lower**).

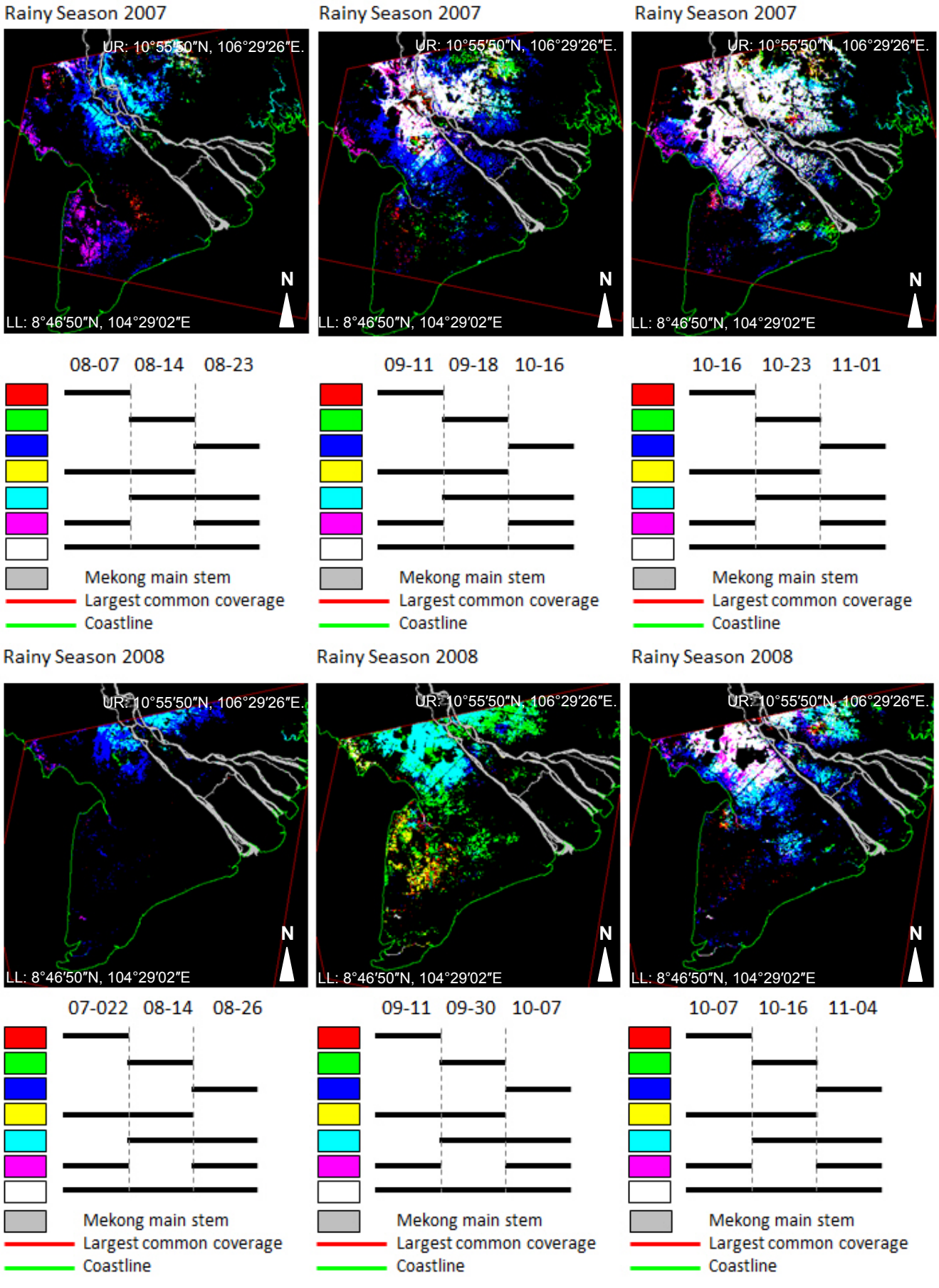

Figure 11 presents patterns of flood progression for the two comparable time series of 2007 and 2008. In 2007 a total of 15 observations were available. In the color display of Figure 11 three composites were generated which show flood progression over the course of three consecutive observations. Please note that near exact dates can be compared. The three binary data sets are stacked, and displayed in RGB (red, green, blue) mode. In this way, areas which are only flooded during the first observation appear red; areas which are exclusively flooded during the second observation appear green, and areas flooded only during the last observation appear blue. According to additive color theory, areas which are flooded during the first two observations (red + green) appear yellow; areas flooded during the last two observations (green + blue) appear cyan, and areas flooded during the first and last (red + blue) observation appear magenta. If an area is flooded three times consecutively it appears white (red + green + blue). For 2007 three triplets are shown: covering the month of August, mid-September to mid-October, and the second half of October, respectively. We can depict how floodwaters progress from north to south and expand radially from the main river. The northern areas of the delta are always flooded. Similar patterns can be observed in three selected triplets of 2008. Comparing 2007 and 2008 it is obvious that in 2007 floodwater extent (especially at the onset in August) was larger, and flooding occurred slightly earlier.

Please note that in each of the triplets dates are chosen that enable comparison between 2007 (upper row) and 2008 (lower row).

5.4. Impact of Dykes on Floodwater Distribution and Progression

As mentioned before, floodwater distribution in the Mekong Delta is influenced by anthropogenic forcing. Farmers control the floodwaters via dykes, and the operation of sluice gates and pumps.

Figure 12 shows the effectiveness of different types of dykes. In An Giang semi-protected and fully protected dykes exist. They vary in height and stability. Fully protected dykes are dykes which managed to fend off water during the century flood in the year 2000, while semi-protected dykes are lower and not as solid. The results show that areas located behind fully protected dykes (pink) are much less often flooded than areas behind semi-protected dykes (green). An Giang is famous for rice production and has converted many areas to three-crop farms. Strict inundation and floodwater control within the dyke systems led to a fourfold increase in rice yield within only the past 40 years [40]. Especially triple rice crop areas are located within high ring dykes. High ring dyke areas are usually provided with higher pumping capacities. According to their findings, areas extensively flooded for longer periods are customarily used for growing two rice crops per year, while strictly controlled fields with shorter flood durations are used for cultivating triple-rice crop systems. For the latter areas farmers prefer varieties with shorter growing periods (≈90 days) compared to varieties of longer growing period in two-season crop areas.

Figure 12. An Giang province in the very north of the Mekong Delta. Fully protected and semi protected dykes (kindly provided by Nguyen Viet Dung) are superimposed on the inundation frequency.

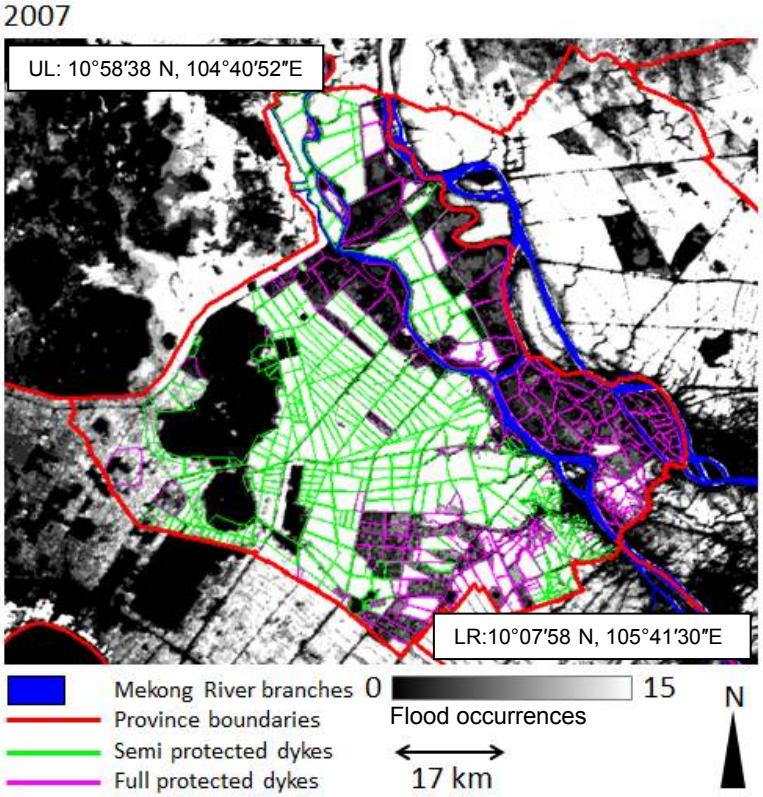

In Figure 13 we depict floodwater progression over the course of the 2007 rainy season within this fully dyked province (Figure 11). Thi Thu Ha *et al.* [40] already underlined that in flood controlled areas gates of dykes are opened about every 3–4 days during the rainy season to flood rice paddy fields—usually before planting the winter-spring rice crop. Based on the results displayed in Figure 13 we can observe that the inundation of compartments with semi-protected dykes or no dykes is controlled by type 1 river floods and overland flow and dyke overflow. In the subsets of time steps 6 and 7 (14 August, 23 August) the flooded area extends rapidly and uncontrollably outside of the protected dyke areas (pink) within un-dyked, and semi-protected (green) dyke areas. Taking a closer look at time steps 7 and 8 (23 August and 11 September), within the turquoise box we can witness how fully protected areas (pink boundary) were intentionally flooded sometime before 23 August, but are non-inundated only two weeks later. Within time steps 9 and 10 (18 September and 16 October) it is depicted how overland and over-dyke flows reach the area of An Giang province, which is furthest away from the Mekong main stem, in the very western corner, between the small hills (pink box). In the same sequence, floodwater control within fully protected dykes (green box) can be observed.

Figure 13. Floodwater progression influenced by the dyke system. Am Giang province, 2007.

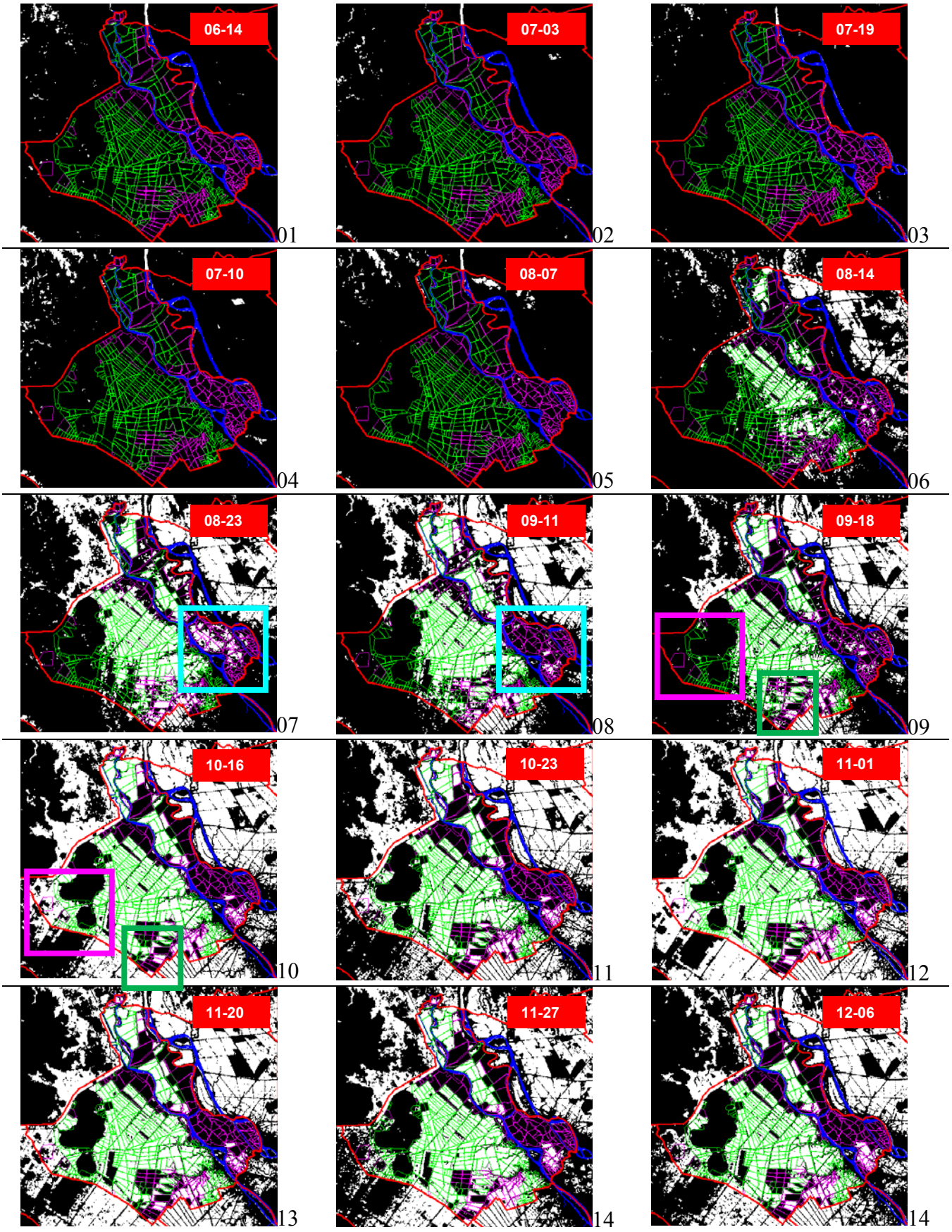

A heated upstream/downstream discussion is not only being led by all Mekong riparians with respect to flood pulse changes induced by hydropower construction or upstream water diversion [37]; this upstream-downstream discourse even takes place within the Vietnamese Mekong Delta. Currently, there is a trend towards areal expansion of triple rice crop systems. However, if more fully protected ring dykes are built this will lead to higher flood hazards downstream in the delta, as a larger amount of water will be pumped out at the falling flood stage. Furthermore, despite the flushing of fields to battle algae, diseases, or accumulated agro-chemicals, the normally stagnant water within dyked fields leads to a complete sedimentation of fertile nutrients. Less sediment reaches downstream localities.

Figure 14. Relationship between land use and flood occurrence, and land use and dykes.

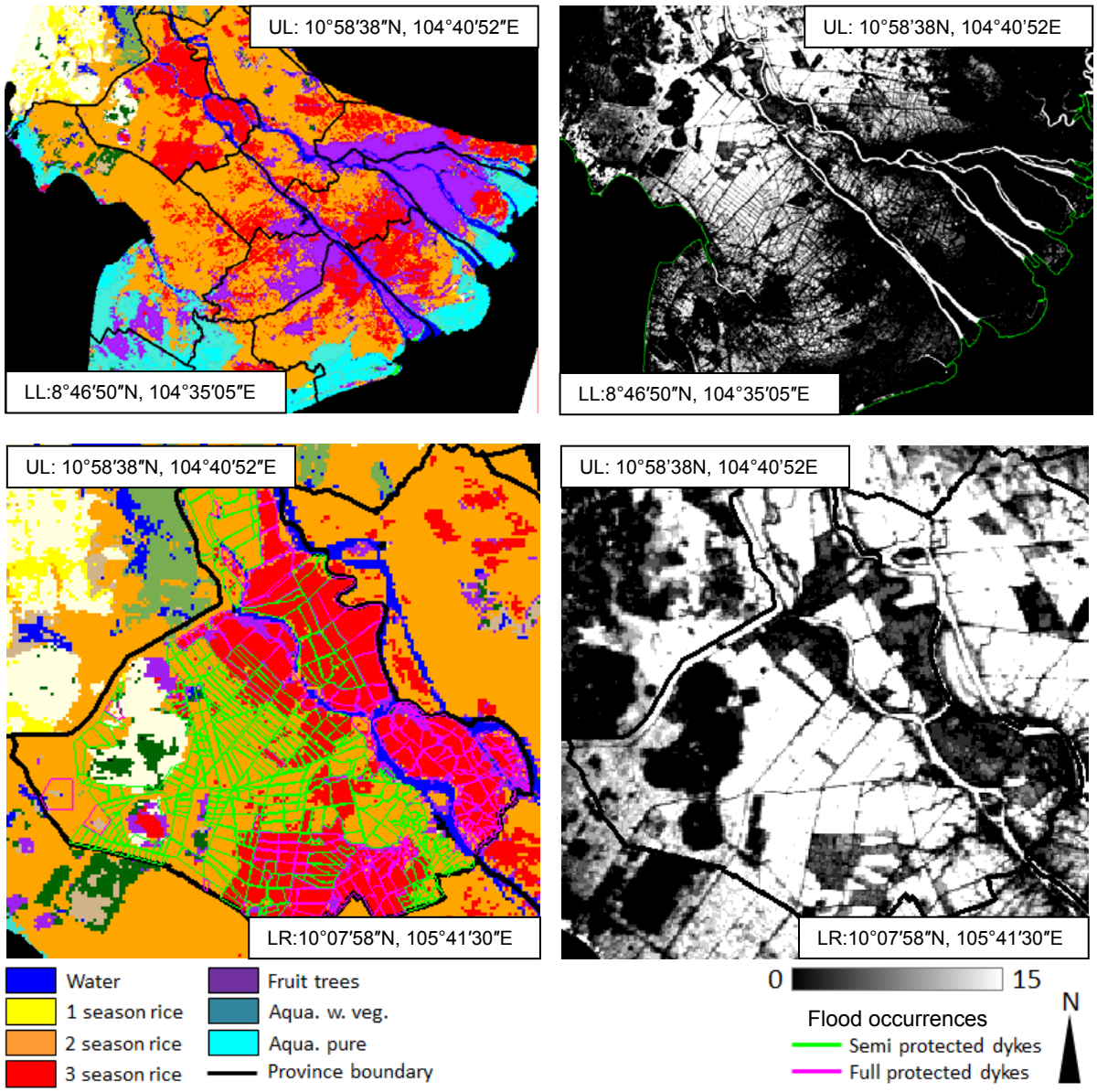

The close relationship of flood patterns, dyke distribution and land use is demonstrated in the following figures. Figure 13 presents a land use classification based on a comprehensive MODIS EVI and reflectance time series at 500 m resolution [56]. As the classification was derived based on the utilisation of over 45,000 MODIS scenes for the whole Mekong Basin, the accuracy and thematic

differentiation for the delta might not be as precise as—for example—a manual classification based on higher resolution data that focuses solely on the delta. However, only phenologic time series analysis really allows the derivation of classes such as one-, two-, and three-season rice crops (yellow, orange, and red), fruit tree orchards (purple), and aquaculture mixed with vegetation (turquoise). There is a clear relationship between land use and flood patterns. The upper part of Figure 14—where the whole delta is presented—depicts that fruit tree orchards (purple) are clearly the regions that are never flooded in the frequency image of 2007 (largest extent of all years). Two-season rice crop regions have the highest flood frequencies and are more often inundated than three-season rice crop areas. The enlarged subset for An Giang province (Figure 14 lower part) underlines this finding. We can show that in this province all areas controlled by full protection dykes (pink lines) are classified as triple rice crop fields, whereas most of the semi-protected dykes encircle two-rice-crop paddies.

6. Discussion

The Mekong Delta has an extremely complex flood regime, and a large amount of earth observation data and ancillary data is needed to visualize, interpret, and understand the driving forces of floodwater occurrence, progression, retreat, and control. So far, only few recent papers have addressed the interwoven topics of Mekong Delta hydrology, diking, and land use. We had the chance to analyse a SAR based time series spanning 60 observations over the course of five years and could shed some light on overall patterns and relations in the Mekong Delta. However, our findings lead to a large set of new questions which cannot all be addressed in the context of this paper. We discuss in the following some major critical points with respect to this study.

Choice of Algorithm

As presented in the introduction numerous publications on water detection algorithms are available. Several algorithms have been compared by different authors, and most water detection algorithms achieve high accuracies and thus—although differing in technique and ancillary data used—do not lead to strongly varying results. For our study it was important to use an algorithm which was available to us (so we used one developed in our group; sources are presented in the introduction). Furthermore, an important criterion for us was the use of an approach not depending on expensive licensed software, so that mapping can also be undertaken by project partners in Vietnam or other relevant countries. The flood maps derived based on our flood detection tool have been validated extensively via comparison with high resolution TerraSAR-X data, with Landsat and Quickbird data, as well as with water land boundary maps. As accuracy of water detection (water surface within the observation scale, and uncovered, compare also below) exceeds 95% [13], we refrained from presenting this data again.

Reliability of Presented Flood Maps

As already stated in the ‘state of the art’ section of the introduction, several external factors influence floodwater detection. Water detection in SAR data is hampered by unfavorable incidence angles (which we did not encounter in this study), by strong wind leading to large waves (also not a

major problem for the flooded areas in the delta), and by vegetation cover above water covered areas. Whereas L-band might provide the chance to assess floodwater beneath tree cover, SAR data acquired at C-band does not allow for the detection of such water surfaces. Luckily, the Mekong Delta has relatively little tree cover. Trees occur as fruit tree orchard plantations especially in the southern part of Can Tho and provinces further to the south. However, these orchard regions are usually located at slightly higher elevation, and floodwaters in the plantation areas are rare. However, there are two other land cover classes where floodwater may occur below tree cover and thus remain un-detected. Firstly, dense mangrove belts exist along the southern and especially south-western and western coast of the delta. Mangroves need brackish water and can survive on flooded ground. However, as the mangrove canopy in these coastal regions is very dense, it is not possible to detect floodwater in these regions. However, as the mangrove areas in the delta are (unfortunately) very small and declining, this does not significantly impair the overall flood detection result. Secondly, floodwater can occur alongside canals whose banks might be overgrown with water hyacinth or *nypa* palms. Also below such vegetation water will not be detectable in SAR data. Due to such areas, where no flood detection algorithm using C-band data can usually recognize water, it is likely that the flood extents presented are rather under- than over-estimated. In many other regions of the world additional DEM data can help to improve flood mapping (simply assuming that a certain terrain height is evenly flooded if not intersected by impenetrable barriers). However, for delta regions of this world this is not feasible, as long as no highly accurate DEM derived from detailed topographic maps or LIDAR air campaigns is available. Global DEMs like SRTM are too coarse in vertical accuracy to be useful for the analysis of flat delta regions. Here, the TanDEM DEM derived from TerraSAR-X data, which is expected to be completed in 2013, might provide one additional data layer to support flood mapping in flat areas.

Observation Scale (Spatial Resolution) of the SAR Data

One topic which urgently needs to be addressed for the Mekong Delta concerns the observation scale for flood mapping. A disadvantage of the—still relatively low—resolution of 150 m is the fact that canals and rivers, which are usually equal or less than 150 m in width, cannot necessarily be extracted. The same applied to flooded areas and flooded fields which are distinctly smaller than 150 m × 150 m. In such areas the radar pixel yields a return signal which represents a mix of different surface properties. If water surfaces are mixed with too many other surfaces (bare soil, infrastructure, vegetation *etc.*) the return signal will be too 'bright' for the flood detection algorithm to accurately retrieve water surfaces. This is, for example, the case in the south-western and southern shoreline areas of the Mekong Delta, which are dominated by aquaculture, as observable in high resolution optical data and determined by *in situ* observations. However, in Figures 5, 6, and 7, the aquaculture ponds located very near the coast of most coastal provinces could not be extracted, as they are much smaller (on average 50 m × 50 m, with other uses, such as orchards, housing, and dry pools, side by side) than the minimum mapping unit of the Envisat ASAR WSM data. The same holds true for small flooded patches within urban areas. In the data presented here, the south-eastern tip of the province of Can Tho, where Can Tho city is located, appears black (never flooded). However, we do know from numerous visits that floodwaters can hamper daily life in Can Tho, and flooded areas of smaller extent occur within and also surrounding the city. These occurrences, though, are also too small to be mapped

by the flood detection algorithm when using ASAR WSM data. As the scope of this study was to understand general flood patterns of the Mekong Delta, this is not of much concern here. It is clear that occurrences which are smaller than the minimum mapping unit can hardly be resolved.

This also affects the mapping of aquaculture. Aquaculture in the delta occurs in natural ponds or artificial pools which are usually far below 30 m × 30 m in size (this would already be a very big aquaculture pond). Aquaculture ponds and pools—even if dominating an area—are separated by smaller agricultural areas, settlements (bright in radar data), mangroves, or shrubland. A 150 m resolved ASAR pixel will thus contain a mix of backscatter from different surface types, and aquaculture is only one part within such a pixel. This is why (see Figure 14) not all aquaculture dominated areas appear as such in the water masks—this is simply a consequence of the size of aquaculture ponds, their density, the types of other surfaces in the area, and the SAR resolution.

As in any remote sensing application there is a limit to the observation scale, and objects which are much smaller than this scale cannot be detected—be they small flooded patches within urban areas, small flood patches within agricultural areas, or aquaculture ponds. Therefore, it is very likely that the flooded area for the Mekong Delta derived from ENVISAT ASAR WSM data is rather under- than over-estimated. To account for this and analyse the degree of this underestimation, in the future we plan to investigate selected areas of the delta based on TerraSAR-X derived inundation time series at 8.25 m and 2.5 m resolutions.

7. Conclusion

Our main findings based on four to five years of Envisat ASAR-WSM derived flood occurrence and flood progression analyses in combination with further ancillary data are:

- Flooding in the Mekong Delta progresses radially from the Mekong branch main stems outwards, as well as from north-west to south-east. In the rainy season floodwaters of type 1 (river flood and overland flow) arrive via Cambodia and spread into the delta. Within the delta, the northern floodplains are inundated the longest, while coastal areas are rarely affected by type 1 flooding. The floods related to the flood pulse of the Mekong, as well as to overland flow in the five years observed, arrive in the Vietnamese Mekong Delta roughly after DOY 215. The high flood stage occurs between DOY 275 and DOY 320. Flood prone provinces such as An Giang, Dong Thap, and Can Tho are flooded to about 40%–50% of the province area during the high flood stage.
- The many different flood types in the delta (river and overland flow, human control, larger rain events, and tidal influences) seriously complicate the interpretation of flood patterns derived from SAR data. Floodwater distribution and timing is not only a complex mix of those four components, but may also be influenced via upstream impacts on the flood pulse. Based on Envisat ASAR WSM time series alone, it is not fully possible to differentiate the individual components, and it is also not possible to distinguish between ‘good flooding’ and ‘bad flooding’. Natural *versus* human induced flooding cannot always be distinguished. However, if ancillary data such as information on land use and dykes are available, interpretation can be more reliable in this respect. A large human-induced control component via dykes and pumping activities can be observed. This fact has to be cautiously considered in all Mekong Delta related

flood modeling. The fused data sets generated here are suitable and have been used for flood model validation and calibration, as it is quite rare to have model evaluation data available that is multi-temporal in nature [35,42].

- Areas which are most often flooded coincide with two season rice crop areas in the delta. They are often located behind semi-protected lower dykes, and also experience overland flooding, such as depicted for An Giang Province. Triple rice crop areas show lower inundation frequencies than double crop areas, and are usually located behind fully protected dyke systems. Concerning the overall delta (dyke data were not available everywhere, but land use data were available) we observed the same pattern: double rice crop areas show a higher inundation frequency than triple crop areas. Regions in the delta which are hardly ever detected as flooded coincide with extensive fruit tree orchards. It is uncommon for orchard regions to flood. However, the problem of water detection below forest canopy exists, and this definitely applies to some small coastal mangrove belt areas (e.g., south-western Ca Mau province), where crown closure of mangroves is too dense for the C-band spectrum of Envisat ASAR to penetrate. However, these really 'forested' areas in the delta are relatively rare—most of the delta is a flat, open agricultural plain. Nevertheless, the fact that some water surfaces lead us to the conclusion that the flood area we present here is rather under- than over-estimated.
- Envisat ASAR WSM analysis is limited by insufficient data availability for true time series analysis. Even though all available data for five consecutive years were derived from the archives of the European Space Agency, ESA, actually only a small fragment covering only two of 13 delta provinces remains for a real time-series analysis of five years. Nevertheless, a current large challenge for the earth observation community is SAR data availability. With the recent failure of the European Envisat in April 2012, the foregoing failure of the Japanese 'Advanced Land Observation satellite', ALOS, in April 2011, the fact that Canadian Radarsat data is quite costly, and that Italian COSMO-SkyMed and German TerraSAR-X data are usually not available at large areal coverage for scientific purposes (also have only been in orbit only since 2007), complicates the current observation of flooded areas. While daily optical data from NOAA-AVHRR and MODIS might yield a chance to circumvent the cloud cover problem in cloud-prone areas, the resolution of 1 km to a maximum of 250 m often has proven to be too low for sufficient flood mapping. The launch of ESA's Sentinel 1 is therefore urgently awaited.

The data and data products derived for this study are available in a web based information system [51,53] to which German and Vietnamese project partners of the WISDOM project [52] have full access, and to which access can be given to further interested scientists upon request and individual evaluation.

Acknowledgements

The authors thank the German Ministry of Education and Research, BMBF, for funding the WISDOM project. Further thanks go to the European Space Agency, ESA, for the free provision of Envisat ASAR WS data. We acknowledge the provision of dyke data for the province of An Giang by Nguyen Viet Dung. Very special thanks go to Trin Thi Long and Vo Khac Tri of the Southern Institute of Water Resources Research, SIWRR, in Vietnam for their support with numerous field campaigns

and for sharing their extensive knowledge on the Mekong Delta. We are also thankful for the constructive comments of four anonymous reviewers.

References

1. Werle, D.; Martin, T.C.; Hasan, K. Flood and coastal zone monitoring in Bangladesh with Radarsat ScanSAR: Technical experience and institutional challenges. *John Hopkins APL Tech. Digest* **2001**, *21*, 148–154.
2. Jonkman, S.N. Global perspectives on loss of human life caused by floods. *Nat. Hazards* **2005**, *34*, 151–175.
3. Long, N.T.; Trong, B.D. Flood Monitoring of Mekong River Delta, Vietnam using ERS SAR Data. Presented at *the 22nd Asian Conference on Remote Sensing*, Singapore, 5–9 November 2001.
4. Kussul, N.; Shelestov, A.; Skakun, S. Flood Monitoring from SAR Data. In *Use of Satellite and In situ Data to Improve Sustainability*; Springer: Heidelberg, Germany, 2011; pp. 19–29.
5. Tholey, N.; Clandillon, S.; De Fraipont, P. The contribution of spaceborne SAR and optical data in monitoring flood events. Examples in northern and southern France. *Hydrolog. Process.* **1997**, *11*, 1409–1413.
6. Hoque, R.; Nakayama, D.; Matsuyama, H.; Matsumoto, J. Flood monitoring, mapping and assessing capabilities using RADARSAT remote sensing, GIS and ground data for Bangladesh. *Nat. Hazards* **2010**, *58*, 525–548.
7. Leinenkugel, P.; Kuenzer, C.; Dech, S. Comparison and optimisation of MODIS cloud mask products for South East Asia. *Int. J. Remote Sens.* **2013**, accepted.
8. Zhou, C.; Luo, J.; Yang, C.; Li, B.; Wang, S. Flood monitoring using multi-temporal AVHRR and RADARSAT imagery. *Photogramm. Eng. Rem. Sensing* **2000**, *66*, 633–638.
9. Richards, J.A.; Woodgate, P.W., Skidmore, A.K. An explanation of enhanced radar backscattering from flooded forests. *Int. J. Remote Sens.* **1987**, *8*, 1093–1100.
10. Hess, L.L.; Melack, J.M.; Filoso, S.; Wang, Y. Delineationg of Inundated Area and Vegetation along the Amazon Floodplain with the SIR-C Synthetic Aperture Radar. *IEEE Trans. Geosci. Remote Sens.* **1995**, *33*, 4, 896–904.
11. Hess, L.L.; Melack, J.M.; Novo, E.M.L.M.; Barbosa, C.C.F.; Gastil, M. Dual-season mapping of wetland inundation and vegetation for the central Amazon basin. *Remote Sens. Environ.* **2003**, *87*, 404–428.
12. Henry, J.-B.; Chastanet, P.; Fellah, K., Desnos, Y.-L. Envisat multi-polarized ASAR data for flood mapping. *Int. J. Remote Sens.* **2006**, *27*, 1921–1929.
13. Gstaiger, V.; Gebhardt, S.; Huth, J.; Wehrmann, T.; Kuenzer, C. Multi-sensoral and automated derivation of inundated areas using TerraSAR-X and ENVISAT ASAR data. *Int. J. Remote Sens.* **2012**, *33*, 7291–7304.
14. Pierdicca, N.; Pulvirenty, L.; Chini, M.; Guerriero, L.; Candela, L. Observing floods from space: Experience gained from COSMO-SkyMed observations. *Acta Astronautica*. **2013**, *80*, 122–133.
15. Matgen, P.; Hostache, R.; Schumann, G.; Pfister, L.; Hoffman, L.; Svanije, H.H.G. Towards and automated SAR based flood monitoring system: Lessons learned from two case studies. *Phys. Chem. Earth* **2011**, *36*, 241–252.

16. Pulvirenti, L.; Pierdicca, N.; Chini, M.; Guerriero, L. An algorithm for operational flood mapping from Synthetic Aperture Radar (SAR) data using fuzzy logic. *Nat. Hazards Earth Sci.* **2011**, *11*, 529–540.
17. Martinis, S.; Twele, A.; Voigt, S. Towards operational near-real time flood detection using a split-based automatic thresholding procedure on high resolution TerraSAR-X data. *Nat. Hazards Earth Syst. Sci.* **2009**, *9*, 303–314.
18. Martinis, S.; Twele, A.; Voigt, S. Unsupervised extraction of flood-induced backscatter changes in SAR data using Markov image modeling on irregular graphs. *IEEE Trans. Geosci. Remote Sens.* **2011**, *49*, 251–263.
19. Mason, D.C.; Speck, R., Devereux, B. Flood detection in Urban Areas using TerraSAR-X. *IEEE Trans. Geosci. Remote Sens.* **2010**, *48*, 882–893.
20. Mason, D.C.; Davenport, I.J.; Neal, J.C.; Schumann, G.J-P.; Bates, P.D. Near Real-Time Flood Detection in Urban and Rural Areas Using High-Resolution Synthetic Aperture Radar Images. *IEEE Trans. Geosci. Remote Sens.* **2012**, *50*, 3041–3052.
21. Kuehn, S.; Benz, Hurley, J.; Hurley, U. Efficient Flood Monitoring Based on RADARSAT-1 Images Data and Information Fusion with Object-Oriented Technology. In *Proceedings of IEEE International Conference on Geoscience and Remote Sensing Symposium (IGARSS '02)*, Toronto, ON, Canada, 22–27 July 2002; Volume 5, pp. 2862–2864.
22. Schumann, G.; Matgen, P.; Hoffman, L.; Hostache, R.; Pappenberger, F.; Pfister, L. Deriving distributed roughness values from satellite radar data for flood inundation modelling. *J. Hydrol.* **2007**, *344*, 96–111.
23. Pulvirenti, L.; Chini, M.; Pierdicca, N.; Guerriero, L.; Ferrazzoli, P. Flood monitoring using multi-temporal COSMO-SkyMed data: Image segmentation and signature interpretation. *Remote Sens. Environ.* **2011**, *115*, 990–1002.
24. Chaouch, N.; Temimi, M.; Hagen, S.; Weishampel, J.; Medeiros, S.; Khanbilvardi, R. A synergetic use of satellite imagery from SAR and optical sensors to improve coastal flood mapping in the Gulf of Mexico. *Hydrolog. Process.* **2011**, *26*, 1617–1628.
25. Kasischke, E.S.; Smith, K.B.; Bourgeau-Chavez, L.L.; Romanowicz, E.A.; Brunzell, S.; Richardson, C.J. Effects of seasonal hydrologic patterns in south Florida wetlands on radar backscatter measured from ERS-2 SAR imagery. *Remote Sens. Environ.***2003**, *88*, 423–441.
26. Kiage, L.M.; Walker, N.D.; Balasubramanian, S.; Babin, A.; Barras, J. Applications of Radarsat-1 synthetic aperture radar imagery to assess hurricane-related flooding of coastal Louisiana. *Int. J. Remote Sens.* **2005**, *26*, 5359–5380.
27. Lang, M.W.; Kasischke, E.S.; Prince, S.D.; Pittman, K.W. Assessment of C-band synthetic aperture radar data for mapping and monitoring Coastal Plain forested wetlands in the Mid-Atlantic Region, USA. *Remote Sens. Environ.* **2008**, *112*, 4120–4130.
28. Martinez, J.M.; Le Toan, T. Mapping of flood dynamics and spatial distribution of vegetation in the Amazon floodplain using multitemporal SAR data. *Remote Sens. Environ.* **2007**, *108*, 209–223.
29. Oberstadler, R.; Hoensch, H.; Huth, D. Assessment of the mapping capabilities of ERS-1 SAR data for flood mapping: a case study in Germany. *Hydrolog. Process.* **1997**, *11*, 1415–1425.

30. Siqueira, P.; Chapman, B.; McGarragh, G. The coregistration, calibration, and interpretation of multiseason JERS-1 SAR data over South America. *Remote Sens. Environ.* **2004**, *90*, 536–550.
31. Townsend, P.A. Mapping seasonal flooding in forested wetlands using multi-temporal radarsat SAR. *Photogramm. Eng. Rem. Sens.* **2001**, *67*, 857–864.
32. Sakamoto, T.; Van Nguyen, N.; Kotera, A.; Ohno, H.; Ishitsuka, N.; Yokozawa, M. Detecting temporal changes in the extent of annual flooding within the Cambodia and the Vietnamese Mekong Delta from MODIS time-series imagery. *Remote Sens. Environ.* **2007**, *109*, 295–313.
33. Kuenzer, C.; Campbell, I.; Leinenkugel, L.; Roch, M.; Dech, S. Understanding upstream-downstream relations in the Mekong Basin in the context of hydropower developments. *Sustainability Science* **2012**, *11*, doi: 10.1007/s11625-012-0195-z.
34. Västilä, K.; Kummu, M.; Sangmanee, C.; Chinvanno, S. Modeling climate change impacts on the flood pulse in the Lower Mekong floodplains. *J. Water Clim. Chang.* **2010**, *1*, 67–86.
35. Nguyen, V.D. Multi-Objective Automatic Calibration of Hydrodynamic Models—Development of the Concept and an Application in the Mekong Delta. Ph.D. Thesis, University of Stuttgart, Stuttgart, Germany, 2011, pp. 177.
36. Ha Nguyen, T.T.; De Bie, C.A.J.M.; Ali, A.; Smaling, E.M.A.; Chu, T.H. Mapping the irrigated rice cropping patterns of the Mekong delta, Vietnam, through hyper-temporal SPOT-NDVI image analysis. *Int. J. Remote Sens.* **2012**, *33*, 415–434.
37. Kuenzer, C.; Knauer, K. Remote sensing of rice crop areas—A review. *Int. J. Remote Sens.* **2012**, in print.
38. Kuenzer, C.; Bluemel, A.; Gebhardt, S.; Vo Quoc, T.; Dech, S. Remote sensing of mangrove ecosystems: A review. *Remote Sens.* **2011**, *3*, 878–928.
39. Vo, Q.T.; Kuenzer, C.; Vo Quang, M.; Moder, F.; Oppelt, N. Review of valuation methods for mangrove ecosystem services. *Ecol. Indic.* **2012**, *23*, 431–446.
40. Huu, N.N. *Flooding in the Mekong River Delta, Viet Nam. Human Development Report 2007/2008*; UNDP Occasional Paper No. 53 within the Program 'Fighting Climate Change'; 2007; p. 23.
41. Renaud, F.; Kuenzer, C. The Water-Development Nexus: Importance of Knowledge, Information and Cooperation in the Mekong Delta. In *The Mekong Delta System—Interdisciplinary Analyses of a River Delta*; Renaud, F., Kuenzer, C., Eds.; Springer: Heidelberg, Germany, 2012; pp. 445–458.
42. Nguyen, N.H.; Delgado, J.M.; Vo, K.T.; Le, M.H.; Merz, B.; Bardossy, A.; Apel, H. Floodplain hydrology of the Mekong Delta, Vietnam. *Hydrolog. Process.* **2011**, doi:10.1002/hyp.8183.
43. Leinenkugel, P.; Esch, T.; Kuenzer, C. Settlement detection and impervious surface estimation in the Mekong delta using optical and SAR data. *Remote Sens. Environ.* **2011**, *115*, 3007–3019.
44. Kuenzer, C.; Liu, G.; Renaud, F.; Ottinger, M.; Dech, S. Asian River Deltas Experiencing Slow-Onset Hazards: Vulnerability, Resilience and Adaptation to Environmental Degradation and Climate Change. In *Proceedings of the International Risk and Disaster Reduction Conference*, Beijing, China, 31 October–2 September 2011.
45. Kuenzer C.; Renaud, F. Climate Change and Environmental Change in River Deltas Globally. In *The Mekong Delta System—Interdisciplinary Analyses of a River Delta*; Renaud, F., Kuenzer, C., Eds.; Springer: Heidelberg, Germany, 2012; pp. 7–48.

46. Vo, K.T. Hydrology and Hydraulic Infrastructure Systems in the Mekong Delta, Vietnam. In *The Mekong Delta System—Interdisciplinary Analyses of a River Delta*; Renaud, F., Kuenzer, C., Eds.; Springer: Heidelberg, Germany, 2012; pp. 49–38.
47. Apel, H.; Nguyen, N.H.; Trinh, T.L.; Vo, K.T. Flood Hydraulics and Suspended Sediment Transport in the Plain of Reeds, Mekong Delta. In *The Mekong Delta System—Interdisciplinary Analyses of a River Delta*; Renaud, F., Kuenzer, C., Eds.; Springer: Heidelberg, Germany, 2012; pp. 221–232.
48. Delgado, J.M.; Merz, B.; Apel, H. Monsoon Variability and the Mekong Flood Regime. In *The Mekong Delta System—Interdisciplinary Analyses of a River Delta*; Renaud, F., Kuenzer, C., Eds.; Springer: Heidelberg, Germany, 2012, pp. 233–245.
49. Leinenkugel, P.; Kuenzer, C., Oppelt, N.; Dech, S. Characterization of land surface phenology and land cover based on moderate resolution satellite data in cloud prone areas—A novel product for the Mekong Basin. *Remote Sens. Environ.* **2013**, accepted.
50. Huth, J.; Gebhardt, S.; Wehrmann, T.; Schettler, I.; Kuenzer, C.; Schmidt, M.; Dech, S. Automated Inundation Monitoring Using TerraSAR-X Multi-Temporal Imagery. In *Proceedings of the European Geosciences Union General Assembly*, Vienna, Austria, 19–24 April 2009.
51. Kuenzer, C. WISDOM: Water related Information System for the Sustainable Development of the Mekong Delta—Thoughts on Sustainability and Long Term Implementation. In *Proceedings of the 3rd Indo-German Conference on Research for Sustainability: Water and Waste Management*, New Delhi, India, 3–4 February 2010.
52. WISDOM. A German-Vietnamese Initiative. Available online: www.wisdom.eoc.dlr.de (accessed on 1 February 2012).
53. Klinger, V.; Wehrmann, G.; Gebhardt, G.; Kuenzer, C. A Water Related Web-Based Information System for the Sustainable Development of the Mekong Delta. In *The Mekong Delta System—Interdisciplinary Analyses of a River Delta*; Renaud, F., Kuenzer, C., Eds.; Springer: Heidelberg, Germany, 2012; pp. 423–444.
54. Gebhardt, S.; Wehrmann, T.; Klinger, V.; Schettler, I.; Huth, J.; Kuenzer, C.; Dech, S. Improving data management and dissemination in web based information systems by semantic enrichment of descriptive data aspects. *Comput. Geosci.* **2010**, *36*, 10, 1362–1372.
55. Vo, Q.T.; Oppelt, N.; Leinenkugel, P.; Kuenzer, C. Remote sensing in mapping mangrove ecosystems—An object-based approach. *Remote Sens.* **2013**, *5*, 183–201.
56. Stone, R. Severe drought puts spotlight on Chinese dams. *Science* **2010**, *327*, 1311.